Biometric Authentication Using Fast Correlation of Near Infrared Hand Vein Patterns

Mohamed Shahin, Ahmed Badawi, and Mohamed Kamel

Abstract—This paper presents a hand vein authentication system using fast spatial correlation of hand vein patterns. In order to evaluate the system performance, a prototype was designed and a dataset of 50 persons of different ages above 16 and of different gender, each has 10 images per person was acquired at different intervals, 5 images for left hand and 5 images for right hand. In verification testing analysis, we used 3 images to represent the templates and 2 images for testing. Each of the 2 images is matched with the existing 3 templates. FAR of 0.02% and FRR of 3.00 % were reported at threshold 80. The system efficiency at this threshold was found to be 99.95%. The system can operate at a 97% genuine acceptance rate and 99.98 % genuine reject rate, at corresponding threshold of 80. The EER was reported as 0.25 % at threshold 77. We verified that no similarity exists between right and left hand vein patterns for the same person over the acquired dataset sample. Finally, this distinct 100 hand vein patterns dataset sample can be accessed by researchers and students upon request for testing other methods of hand veins matching.

Keywords—Biometrics, Verification, Hand Veins, Patterns Similarity, Statistical Performance.

I. INTRODUCTION

ASSOCIATING an identity with an individual is called personal identification. The problem of resolving the identity of a person can be categorized into two types of problems; *verification* and *identification*. Verification (authentication) refers to the problem of confirming or denying a person's claimed identity (Am I who I claim I am?). Identification (Who am I?) refers to the problem of establishing a person's identity. Automatic human identification has become an important issue in today's information and network-based society. The techniques for automatically identifying an individual based on his/her physiological or behavioral characteristics are called *biometrics*, which provides an answer to this need. Biometric techniques fall into two categories: *physiological* and

Manuscript received April 30, 2007. This work was accomplished at Systems & Biomedical Engineering Department, Cairo University, Egypt.

Mohamed Shahin is with Ismaillia Suez Canal Authority Hospital, Egypt (e-mail: mkhairy@hotmail.com).

Ahmed Badawi is a visiting professor with University of Tennessee, Knoxville, Biomedical Engineering Department, 315 Perkins Hall, 1506 Middle Dr., Knoxville, TN, 37996, USA (phone: 865-974-6009; fax: 865-946-1787; e-mail: ambadawi@utk.edu). He is a professor on leave at Systems & Biomedical Engineering Department, Cairo University.

Mohamed Kamel is with Systems & Biomedical Engineering Department, Cairo University, 13216, Egypt (e-mail: sherin_2002@mail.com).

behavioral categories. Common physiological biometrics include face, eye (retina or iris), finger (fingertip, thumb, finger length or pattern), palm (print or topography), and geometry, back of the hand vein pattern or thermal images. Behavioral biometrics includes voiceprints, handwritten signatures, and keystroke/signature dynamics.

Personal verification has become an important and high-demand technique for security access systems in the last decade. Shape of the subcutaneous vascular tree of the back of the hand contains information that is capable of authenticating the identity of an individual [1-5, 22] to a reasonable accuracy for automatic personal authentication purposes. The shape of the finger vein patterns and its use for identification purpose was proposed by Miura et al. [4]. The infrared region is of special advantage since the skin tissue is relatively transparent and the blood absorbs infrared light well. Hence, the veins-background contrast is higher than the visible area. Since the arrival of fairly low cost CCD cameras and computer power, it seems straightforward to try to consider these technologies [6-7]. Normally, black and white CCD cameras are also sensitive in the near infrared region, so a filter blocking the visible light is all that is needed on the camera. Proper lighting is of course essential to obtain even illumination on the skin surface. There are many research attempts for the extraction, segmentation and tracing of subcutaneous peripheral venous patterns [8-11], its main aim is to make data reduction and noise suppression for good diagnostic purposes and for making some quantitative measurements like lengths and diameters for the extracted vessel segments. These techniques are based on mathematical morphology and curvature (veins direction) evaluation for the detection of vessel patterns in a noisy environment. Researchers in hand vein biometrics [1-5, 22] had a satisfactory result for either verification or identification purposes, regardless of the difference in datasets size, methods, or vein similarities used. The vein tree detection stage includes four consecutive sub stages, which are hand region segmentation (i.e. region of interest localization and background elimination), smoothing and noise reduction, local thresholding for separating veins, and postprocessing. In this paper we propose a design of a hand vein biometric authentication system performing a fast spatial correlation method for hand vein patterns matching.

II. DATA ACQUISITION AND PROCESSING

In visible light, the vein structure on the back of the hand is not easily discernible. The visibility of the vein structure varies significantly depending on factors such as age, levels of

subcutaneous fat, ambient temperature and humidity, physical activity, and hand position. In addition a multitude of other factors including surface features such as moles, warts, scars, pigmentation and hair can also obscure the image. Fortunately, the use of thermographic imaging in the near IR spectrum exhibit marked and improved contrast between the subcutaneous blood vessels and surrounding skin, and eliminates many of the unwanted surface features. The temperature gradient between the veins and surrounding tissue is generally more pronounced than the difference that can be seen by the naked eye. A commercially available conventional charge-couple device (CCD) monochrome camera, rather than a considerably more expensive thermal camera, is used to obtain the thermal image of the back of the hand. Though principally designed for use in visible light, CCD cameras are also sensitive to near IR wavelengths of the electromagnetic spectrum up to about 1100 nm. This is an actinic IR range, which covers the near infrared spectrum from 700-1400 nm. A CCD camera that is highly sensitive in the near infrared region was chosen. The camera characteristic curve is shown in Fig. 1. The greatest intensity of IR radiation emitted by the human body is 10 mW/cm^2 and is in the range of 3000-14000 nm [1]. Unfortunately, the CCD camera has no sensitivity in this region. Furthermore any naturally emitted near IR radiation is far too weak to be detected by the camera's CCD imager. Consequently after experimentation with a variety of light sources, including high intensity tungsten lamps, it was found to be necessary to irradiate the back of the hand using an IR cold (solid-state) source. The reduced hemoglobin in venous blood absorbs more of the incident IR radiation than the surrounding tissue thus appearing darker.
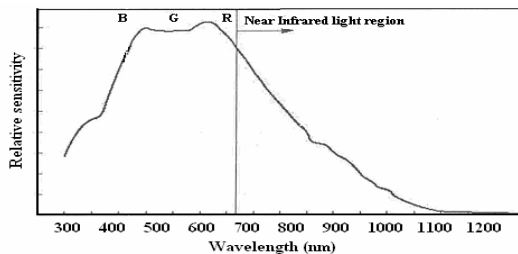

Fig. 1 Spectral sensitivity characteristics of used silicon based CCD sensor

The depth of absorption and radiation of actinic IR in biological tissue is approximately 3 mm, and so thermal IR radiation provides information only about surface (skin) temperatures of biological objects [1]. As a consequence only the subcutaneous vascular network is discernible in the image. The quality and extent of the revealed vein structure is however highly variable. The distinctiveness of the network depends on the thickness of the overlaying skin, on the degree of venous engorgement, on the conditions of the vein walls and on the nearness of the veins to the surface.

In our system, we have designed a near IR cold source to provide back-of-hand illumination. The IR cold source is a solid-state array of 24 LEDs (light emitting diodes). The diodes are mounted in a square shape, 6 LEDs in each side, on

a designed and assembled PCB (printed circuit board). We made a housing and an attachment for fixing the LEDs around the CCD lens. Our experiments showed that the cold source provides better contrast than the ordinary tungsten filament bulbs. A commercially available, low cost, monochrome CCD fitted with an IR filter is used to image the back of hand. The transmission curve for the used filter (Hoya RM90) is shown in Fig. 2. The curve reveals that the filter has a small tail of transmittance down to about 750 nm.
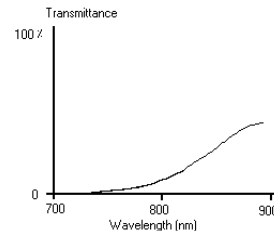

Fig. 2 Transmission curve for the RM90 Hoya IR filter

The IR filter ensures that no visible light reaches the CCD sensor. After using the cold IR light source and the IR filter, the image constructed on the CCD sensor is totally a thermal graph for the back of the hand. The mostly distinguishable component in the image is the superficial vein tree pattern as shown in Fig.3 to the right. A comparison between visible light image and infrared image for the same person's hand is demonstrated in Fig. 3.

A simplified schematic diagram for our hand vein image acquisition prototype module is demonstrated in Fig. 4. As in Fig.3 to the left, the hand is presented as a clenched fist with the thumb and all the other fingers are hidden. It allows a person to easily position his/her hand in front of the camera and it eases the shape matching search process (translation and rotation variations).
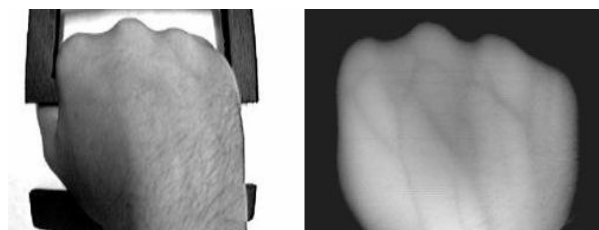

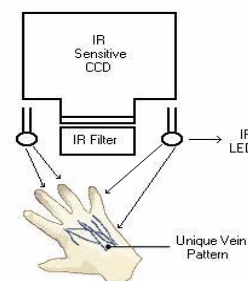Fig. 3 Visible light image (left) and IR image (right) for the same person

Fig. 4 Schematic of the hand vein pattern imaging module

The intensity of IR source is attenuated by the use of diffusing paper and it helps for obtaining an equally distributed illumination on the hand area. A monochrome frame-grabber is used to capture an image of the back of a hand for computer processing. Images are captured using a 320W X 240H pixels video digitizer with a gray-scale resolution of 8-bits per pixel.

A sample hand vein image from our data set is shown in Fig. 5 for a male hand. A dataset of 50 persons of different ages above 16 and of different gender, each has 10 images per person was acquired at different intervals, 5 images for left hand and 5 images for right hand. The data set is for normal persons who do not complain from any diseases such as arthritis.
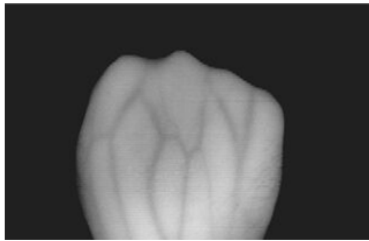

Fig. 5 Acquired image of 320W x 240H pixels, 8-bits per pixel

A. Hand Vein Image Processing Stages

This is the second stage in the Hand Vein Verification System (HVVS) after the acquisition, which covers the detection of vein structures from the acquired infrared image for the back of the hand. The vein tree detection stage includes four steps, which are hand region segmentation (i.e. region of interest localization and background elimination), smoothing and noise reduction, local thresholding for separating veins, and finally the postprocessing. Fig. 6. illustrates the block diagram of the processing stage.
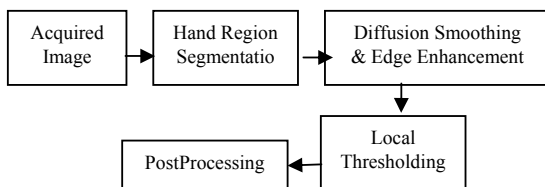

Fig. 6 Block diagram of hand veins processing stage

B. Hand Region Segmentation

Image segmentation is one of the most important steps leading to the analysis of processed image data. Its main goal is to divide an image into parts that have a strong correlation with objects or areas of the real world contained in the image.

Binarization is the case of segmenting the image into two levels; object (hand region) and background; the object segment which is the region of interest (ROI) in white and the background segment in black as shown in Fig. 7. The algorithm used in the segmentation sub stage is an iterative method used for calculating and selecting an optimal threshold, which is used to segment the image into two distinct parts; hand and background [13]. We used this

resultant binary image to calculate the center of gravity (COG) for our ROI (hand region). Then we translated the grayscale hand region to the center of the image after assigning the background area to zero gray value pixels. Thus we completely localized, separated and centered the hand region for subsequent processing steps.

Fig. 7 Segmentation results; (a) Input gray scale image (b) Binary image and (c) Output image after ROI determination and centering

C. Smoothing and Noise Reduction

Two approaches could be used for noise filtering. First approach is using Gaussian smoothing filter. The disadvantage of Gaussian filter is its non-edge preserving ability, since it blurs the image with equal weights; also edges of the veins are blurred and completely diffuse after performing several smoothing iterations. The second approach is an edge-preserving technique like nonlinear diffusion [16-17]; in which the image gradient was used to weight the diffusion process. Fig. 8 show results of the smoothing filters used on three line profiles, where we used a median filter of 5*5 mask in order to remove the hand traces from the acquired image then we used the nonlinear diffusion filter based on edge weighted diffusion in order to smoothen the image while preserving the vein edges. The smoothing and noise removal sub stages effect is shown in Fig. 8 for 5 iterations of nonlinear diffusion of optimized diffusion parameters for these images, while the edges are not affected.
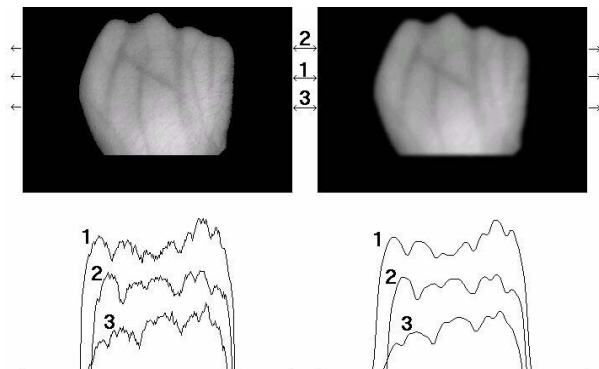

Fig. 8 Effect of smoothing sub stage on the three image line profiles

D. Hand Vein Pattern Segmentation

Hand vein segmentation is specifically to divide a hand vein image into a foreground (veins in the back of the hand) and a background (non-vessel areas). Segmentation methods can be divided into four groups, which are threshold-based segmentation, edge based segmentation, and region based segmentation and segmentation by matching. In this work, the

first thresholding method is adopted since it is computationally inexpensive. Considering that we want to process and study veins only, global thresholding (i.e. single threshold for the whole image) is not a good technique for this purpose. A better approach is to calculate the average around each pixel of the image in an area of NxN neighbor pixels and to use average value as a threshold value [11]. The local threshold process separates the vein pattern from the background; hence the desired vein image is extracted. Experimentally and after optimization, we have chosen a 31x31 mask size for computing the threshold for binarizing the central pixel. The result is shown in Fig. 9.
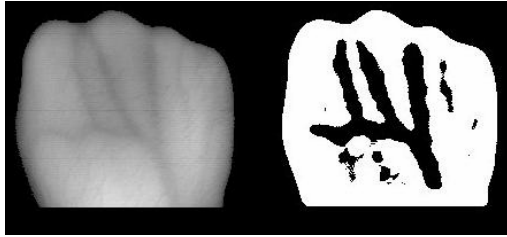

Fig. 9 Processed image (left) and its local thresholded image (right)

E. Hand Vein Pattern Postprocessing

It is demonstrated from Fig. 9 that the resultant binary hand vein contains some noise and un-sharp edges. We experimentally applied 5x5 median filter for improving and validating the output binary hand vein pattern and for reducing the effect of these unwanted defects. We also converted the vein pattern into white in a black background which in this case the entire image. The final pattern after the post processing sub stage is shown in Fig. 10.
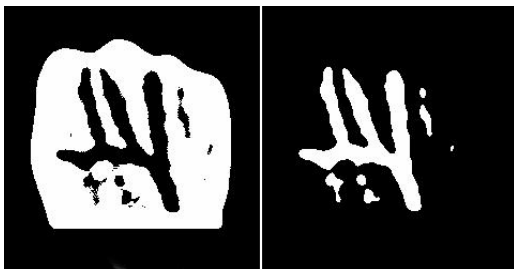

Fig. 10 Hand vein pattern before (left) and after postprocessing (right)

F. Matching of Hand Vein Patterns

The ordinary use of the designed hand attachment does not allow rotational degrees more than -15 to 15 and translations in X and Y more than -35 pixels to 35 pixels. After image acquisition and hand vein extraction sub stages, we have a binary image that contains the segmented back of the hand vein pattern. This is suitable for the next and the final sub stage, the matching of hand vein patterns. The input for the matching sub stage is two binary hand vein images like the one in Fig. 10 (right), the matching output is Yes (the two images are for the same pattern) or No (the input images are not correlated). We used rigid registration technique [14] since we already constrained our data acquisition system with

the attachment in order to prevent any large translation or rotation. One of the two images is remained stationary while we apply 2D transformation (x-translation, y-translation and rotation) on the other image in order to align it with the first pattern (Registration) to find the maximum correlation percentage between two hand vein images as in equations 1-2.

$$Correlation(Tx, Ty, \theta) = \underset{Tx, Ty, \theta}{Forall} (|X \bullet T| * 100) / Min(|X|, |T|) \quad (1)$$

$$MaxCorrelation = Max(Correlation(Tx, Ty, \theta)) \quad (2)$$

Where X in equation 1 is an image which contains the first test binary hand vein pattern, T is the second image which contains the transformed template binary hand vein pattern, $\bullet$ is the logical AND operator, || operator is the summation of ones in the matrix. |X| equals the number of ones in the X image pattern, Min ($|X|, |T|$) is the minimum count of the white pixels between the two patterns to be matched. However Fujitsu researchers have presented a contactless/touchless palm vein authentication which is more convenient and non hygienic for users, we restricted our research designed prototype for a contact system type in order to simplify our matching phase and derive a dependent statistical measures for this proposed prototype. However accounting for scale (Age or hand to camera distance) in the registration algorithm is simple, we did not account for the scale in our matching since the distance from hand to camera is fixed and we assume that the real biometric system capture a new template each time interval. In real systems, capturing the hand template at equal monthly intervals after correct authentication is suggested in order to track the changes in the hand with age. The matching (similarity) percentage is calculated as the ratio of the count of overlapped white pixels between input images to the number of white pixels in one of the two input images (the image with the minimum count of the white pixels). We calculated the matching ratio for each transformation step then we choose the maximum ratio as the final matching ratio between the two input hand vein patterns. In our fast implementation and for saving time of matching, we made the parameters (x-translation, y-translation, and rotation) steps equals 5, getting the maximum matching ratio on this grid, finally we made a fine search (tune pixel by pixel and 0.5 degree) to find the overall maximum correlation ratio. The result of matching sub-stage is shown in Fig. 11. A case of correct true match is demonstrated. The resultant pattern is correlated to the input images and it is shown that the matching ratio is 81.87 % (same person). A case of correct mismatch is shown in Fig. 12, the matching ratio is small as 48.27 % (different persons).
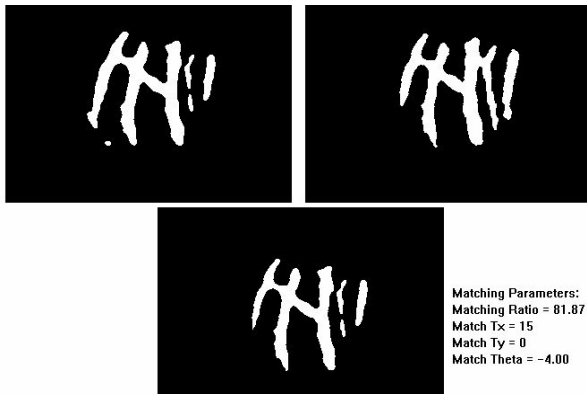
Matching Parameters:
Matching Ratio = 81.87
Match Tx = 15
Match Ty = 0
Match Theta = −4.00

Fig. 11 Example of true match for different patterns (left and right) of the same person and its associated high correlation (bottom)

Matching Parameters:
Matching Ratio = 48.27
Match Tx = 1
Match Ty = 10
Match Theta = −15.00
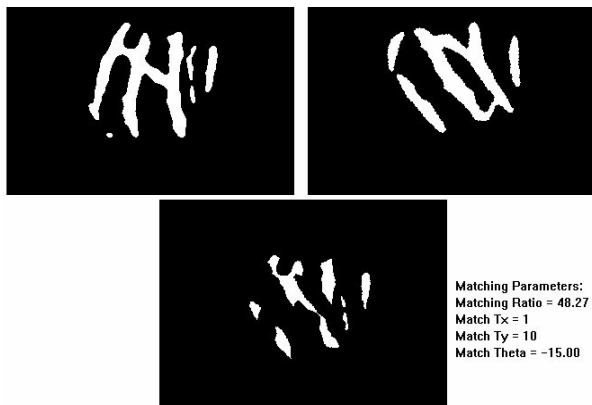
Fig. 12 Example of correct mismatch between different persons (left and right) and its associated low correlation (bottom)

III. RESULTS

A. Overall Performance

The system was tested over a dataset collected using the designed system consisting of 50 persons of different age and gender for each 5 left and 5 right images were acquired. The person was asked to put his/her right hand on the hand attachment frame and the system operator captures the first image for the current person right hand veins. Then the person replaces his/her right hand with the left one for acquiring the first image for the left hand vein pattern. This process was repeated until we acquire five images for the right hand and five images for the left hand in different scenes (5 minutes interval between every acquired image) independent of each other, i.e. ten images for each person. We will prove in our statistical analysis that the hand vein pattern is unique to some level for each person and for each hand. Thus we considered as if we have 100 persons of which 5 images are in the dataset since we found that the left and right hand vein images are different. In order to find the dissimilarity threshold in correlation ratio between the 100 hands we have chosen only the first image pattern for each of the 100 hands and for a correlation ratio threshold that exceed 80%, we achieved 100% classification (Distinct pattern). For evaluating the uniqueness of the vein patterns, all possible

comparisons are made between the whole data. We matched each image from our data set with all the 500 hand vein images in our dataset and then we recorded the matching ratios. We constructed the correlation matrix for representing the matching result between each image and all other images. We performed statistical analysis for selecting an optimal threshold to get the highest system performance, by testing the system over the whole dataset. To evaluate the hand vein performance, we used measures of performance, which include: sensitivity, specificity, false accept rate (FAR), false reject rate (FRR), and efficiency. Fig. 15 shows graphically how FAR(%), and FRR (%) change with different thresholds. Our aim is to select an optimal threshold. We want a single criterion, such that it takes into account the maximization of true events (GAR, GRR) and minimization of error events (FAR, FRR). Fig. 13 illustrates the change of system performance at different thresholds. Efficiency, which we will consider as our criterion for evaluating the system performance at different thresholds, reaches its maximum of about 99.88% at a threshold of 78. At this threshold the Sensitivity is 92.16%, the Specificity is 99.97%, FAR is 0.03%, and FRR is 7.84%. Receiver Operating Characteristic (ROC) curve is shown in Fig. 14. A receiver operating curve provides an empirical assessment of the system performance at different operating points which is more informative than FAR and FRR.
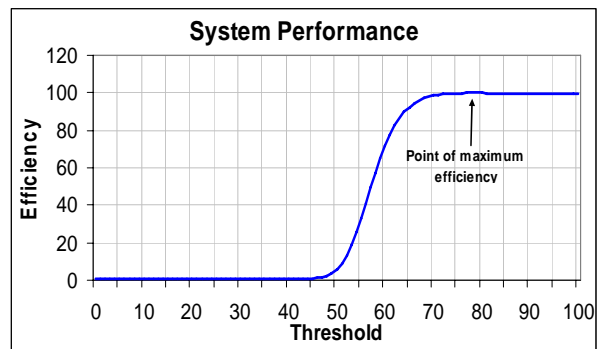

Fig. 13 System Performance (Efficiency) at different thresholds
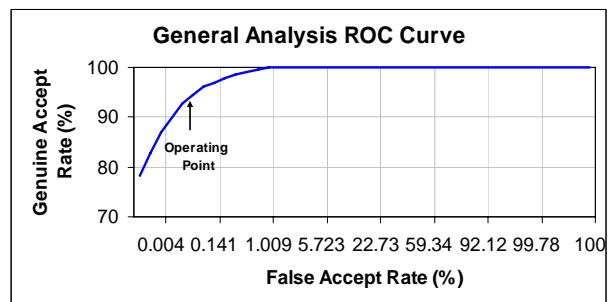

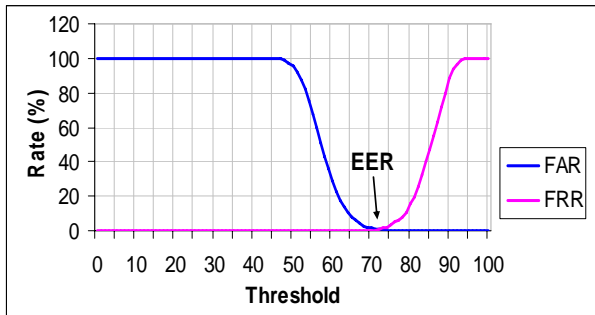Fig. 14 General analysis receiver operator characteristic curve (ROC)

Fig. 15 FRR (Type I Error) versus FAR (Type II Error)

Hand Vein Verification System (HVVS) is accurate in the low to medium security level: e.g., for a threshold 75, the genuine acceptance rate is 96.72% for only a 0.18% FAR. Although the 0.18% FAR may seems high, in practice it is much smaller, since a user of the system does not know the identity of which other users can claim that their hand veins match. Fig. 15 demonstrates FAR(%) and FRR(%) curves on the same graph. To get around this, vendors often provide a variable threshold setting, which allows the customer to strike a balance. If a site needs near 100% rejection of impostors, authorized users will have to pay for some % rejection rate.

A commonly used point to examine the quality of performance is to evaluate Equal Error Rate (EER) point and it assumes that the costs of FA and FR are equal, and that the class prior probabilities (of client and impostor distributions) are also equal. From Fig. 15, we obtained an ERR for the test data = 0.695% at Threshold = 72.

B. Similarity between Right and Left Patterns

A previous study on the individuality of biometric signal such as fingerprint was performed in [18] in order to prove the uniqueness of fingerprint features. In the previous section we proved that the hand vein pattern is unique to some extent for each identity (person), in this section we will estimate the probability for the true match between the right and left hand vein patterns for the same identity. If this probability is low, we will decide that the hand vein patterns are unique for each identity and are unique for each hand i.e. the hand vein pattern for the right hand is different from the hand vein pattern for the left hand of the same person. Else if the resultant estimated probability value is large, we will conclude that the hand vein patterns are unique for each identity but not unique for each hand.

Using the correlation matrix, we calculated the mean and standard deviation for the matching ratios between the right and left hand vein pattern for the same person [15]. We calculated the probability for the matching ratio to be greater than the threshold we determined in the previous section. The probability of the matching ratio to be greater than 78% (for deciding a true match), is the probability for the two hands (right and left) for the same person to have a similar vein pattern. Table I shows the probability values for the thresholds displayed in the range from 70% to 80%. The probability at the threshold that gave us the maximum efficiency in the

previous section (78%) is: Probability (Similarity >= 78%) = 0.0002.

TABLE I
STATISTICAL RESULTS FOR THE PERFORMANCE OF THE SYSTEM, PROBABILITY FOR THE TRUE MATCH BETWEEN THE RIGHT AND LEFT HAND VEIN PATTERNS FOR THE SAME IDENTITY

Threshold	MEAN	Std. Dev.	$Z = $ (Threshold -Mean)/ Std.Dev.	P(Z)	0.5-P(Z)	P(Similarity >= Threshold) %
70	58.106	5.531	2.149	0.4842	0.0158	1.58
71	58.106	5.531	2.329	0.4901	0.0099	0.99
72	58.106	5.533	2.510	0.4940	0.0060	0.6
73	58.106	5.533	2.691	0.4964	0.0036	0.36
74	58.106	5.533	2.872	0.4979	0.0021	0.21
75	58.106	5.533	3.052	0.4989	0.0011	0.11
76	58.106	5.533	3.233	0.4994	0.0006	0.06
77	58.106	5.533	3.414	0.4997	0.0003	0.03
78	58.106	5.533	3.594	0.4998	0.0002	0.02
79	58.106	5.533	3.775	0.4999	1E-04	0.01
80	58.106	5.533	3.956	0.5	0	0

The calculated probability is small enough to some extent in order to let us conclude that the hand vein patterns are unique for each identity and is unique for each hand i.e. the hand vein pattern for the right hand is different from the left hand for the same person. Fig. 16 shows two hand vein images for the same person, the left one for his left hand and the right one for his right hand.
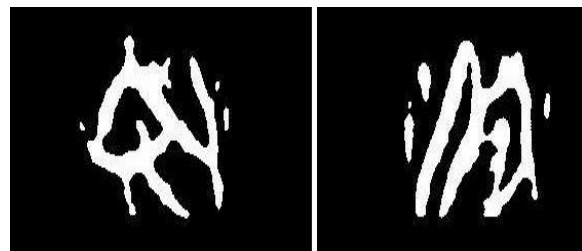

Fig. 16 Two-hand vein patterns for the same person, left and right hand

C. Verification Testing

To obtain the verification accuracy of our system, each of the images was matched with all of the images in the dataset after reducing it to 300 patterns (3 template images for each hand). A matching is noted as a correct matching if two images are from the same hand. The total number of matching is 20000 (200 images* 100 different hands). The probability distributions for genuine and imposter are estimated by the correct and incorrect matching, respectively, and are shown in Fig. 17.

Fig. 18 depicts the corresponding ROC curve, for all possible operating points. From Fig. 18, we can see that our system can operate at a 97 % genuine acceptance rate and a 0.02 % false acceptance rate, and the corresponding threshold is 80. The system's testing equal error rate is 0.25 % at threshold 77. In this verification testing analysis, we used 3 images to represent the templates and 2 images to test. Each image is matched with the existing 3 templates. The same

analysis for the 300*300 as in section A was repeated. Figures 17-19 show the results. For the 300*300 templates, the optimal threshold is 79 with FAR of 0.02% and FRR of 7.22%. For the testing phase, matching the 200 test with the 300 templates of 100 hands, the optimal threshold is 80 with FAR of 0.0202% and FRR of 3.00%. The system efficiency at this threshold was found to be 99.95%. Fig. 19 shows FAR and FRR versus threshold. The EER obtained is 0.25 % at threshold 77.
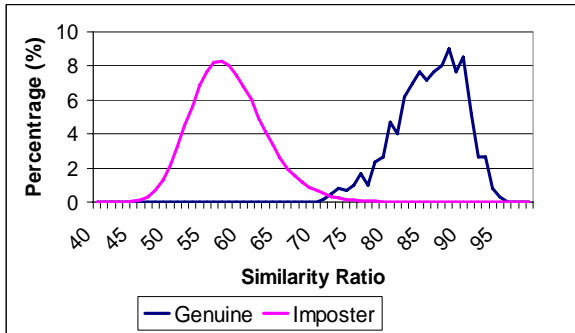

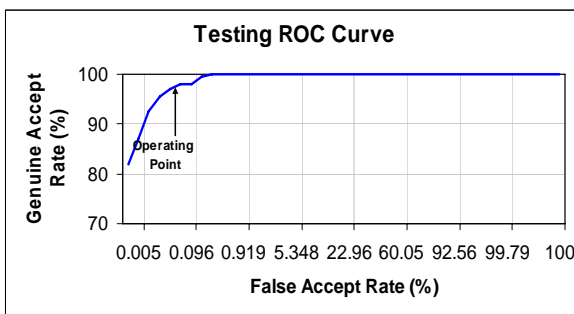Fig. 17 Verification test results for genuine and imposter distributions

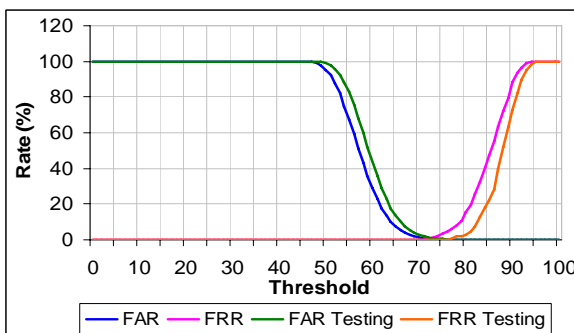Fig. 18 Verification testing, ROC curve

Fig. 19 FAR & FRR for template and test analysis

IV. CONCLUSION

The designed system was tested for verification purpose only over a dataset collected with the designed prototype system. This dataset is for 50 persons of different age and gender of which ten images per person were acquired (five for the right hand and five for the left) in different scenes at different intervals and are independent of each other, i.e. ten images for each person. Verification performance statistical parameters were estimated for the overall system such as: Genuine Accept Rate (Sensitivity), Genuine Reject Rate (Specificity), False Accept Rate (FAR), False Reject Rate (FRR), Efficiency and Receiver Operating Curve (ROC). System overall performance (overall efficiency) was found to be 99.88% at threshold (matching ratio) equal 78. At this maximum efficiency the Sensitivity obtained is 92.16%, the Specificity is 99.97%, FAR is 0.03%, and FRR is 7.84%. For the testing phase, matching the 200 test with the 300 templates of 100 hands, the optimal threshold obtained is 80 with FAR of 0.02% and FRR of 3.00 %. The obtained system efficiency at this threshold is 99.95%. The obtained EER is 0.25% at threshold 77. However the difference in methods, datasets, and algorithms that were found in the hand veins biometric work of [1-4, 21-22], our performance results are comparable. We studied the similarity between right and left hand vein pattern for the same person. We verified that the hand vein pattern is unique for each person and is also unique for each hand based on our hand vein images dataset. Finally, since there is no available dataset for hand vein research purposes, the acquired hand veins dataset considered for 100 distinct hands of 5 images per hand will be available for free upon request for testing other methods to other researchers and students working in biometrics.

REFERENCES

[1] J. M. Cross and C. L. Smith, "Thermographic Imaging of the Subcutaneous Vascular Network of the Back of the Hand for Biometric Identification", *Proceedings of 29th International Carnahan Conference on Security Technology*, Institute of Electrical and Electronics Engineers, pp. 20–35, 1995.

[2] S. Im, H. Park, Y. Kim, S. Han, S. Kim, C. Kang, and C. Chung, "A Biometric Identification System by Extracting Hand Vein Patterns", *Journal of the Korean Physical Society*, vol. 38-3, pp. 268-272, March 2001.

[3] T. Tanaka and N. Kubo, "Biometric Authentication by Hand Vein Patterns" *SICE, Annual Conference in Sapporo*, pp. 249-253, Aug. 2004.

[4] N. Miura, A. Nagasaka, and T. Miyatake, "Feature Extraction of Finger-Vein Patterns Based on Repeated Line Tracking and its Application to Personal Identification", *Machine Vision and Applications*, vol. 15, pp. 194-203, 2004.

[5] C. Lin and K. Fan, "Biometric Verification Using Thermal Images of Palm-Dorsa Vein Patterns", *IEEE Transactions on Circuits and systems for Video Technology* vol. 14, No. 2, February 2004.

[6] O. Such, "Near Infrared Imaging of Hemodynamics", Proceedings of 18th *International Conference of the IEEE/EMBS*, Amsterdam, Nov. 1996.

[7] O. Such, Sabine Acker, and Valdimir Blazek, "Mapped Hemodynamic Data Acquisition by Near Infrared CCD Imaging", *Proceedings of 19th International Conference of the IEEE/EMBS*, Chicago, Oct. 1997.

[8] E. K. Y. Chan and J. A. Pearce, "A Rule-Based, Adaptive Window-Size Filter for the Enhancement of Subcutaneous Vascular Patterns in Thermographic Images", *Proceedings of 11th International Conference of the IEEE/EMBS*, pp. 1746-1748, Oct. 1989.

[9] K. Eric, Y. Chan and J. Pearce, "Visualization of Dynamic Subcutaneous Vasomotor Response by Computer-Assisted Thermography", *IEEE Transactions on Biomedical Engineering*, vol. 37-8, pp. 786-795, August 1990.

[10] K. Eric, Y. Chan and J. Pearce, "A Computer-Assisted Thermography System for the Extraction, Visualization and Tracing of Subcutaneous Peripheral Venous Patterns", *IEEE International Symposium on Circuits and Systems*, vol. 1, pp. 508 –511, 1991.

[11] Y. Sun, "Automatic Identification of Vessel Contours in Coronary Arteries in Arteriograms by an Adaptive Tracing Algorithm", *IEEE Transactions on Medical Imaging*, vol. 8-1, pp. 78-88, March 1989.

[12] F. Van Der Heijden, *Image Based Measurement Systems*, John Wiley & Sons, 1995.

[13] M. Sonka, V. Hlavac, and R. Boyle, *Image Processing, Analysis and Machine Vision*, Chapman & Hall, 1993.

[14] R. Schalkoff, *Pattern Recognition: Statistical, Structural and Neural Approaches*, John Wiley & Sons, 1992.

[15] A. Papolis, *Probability, Random Variables and Stochastic Processes*, Third Edition, McGraw-Hill, New York, 1991.

[16] K. Abd-Elmoniem, A. Youssef, and Y. Kadah, "Real-Time Speckle Reduction and Coherence Enhancement in Ultrasound Imaging via Nonlinear Anisotropic Diffusion", *IEEE Transactions on Biomedical Engineering*, vol. 49-9, pp. 997-1014, 2002.

[17] Ahmed M. Badawi, Muhammed A. Rushdi, "Speckle Reduction in Medical Ultrasound: A Novel Scatterer Density Weighted Nonlinear Diffusion Algorithm Implemented as Neural Network Filter," *Proceedings of the 28th IEEE 2006 International Conference of the Engineering in Medicine and Biology Society (IEEE/EMBS)*, pp. 2776-2782, Aug 30-Sep 3, New York City, USA, 2006.

[18] S. Pankanti, S. Prabhakar, and A. Jain, "On the Individuality of Fingerprints", *IEEE Transactions on Pattern Analysis and Machine Intelligence*, vol. 24-8, pp. 1010-1025, Aug. 2002.

[19] A. Jain, S. Prabhakar, L. Hong, and S. Pankanti, "Filterbank-Based Fingerprint Matching", *IEEE Transactions on Image Processing*, vol. 9-5, pp. 846-859, 2000.

[20] A. Jain, L. Hong, and R. Bolle, "On-Line Fingerprint Verification", *IEEE Transactions on Pattern Anakysis and Machine Intelligence,* vol. 19-4, pp. 302-314, 1997.

[21] R. Sanchez-Reillo, C. Sanchez-Avilla, and A. Gonzalez-Macros, "Biometrics Identification Through Hand Geometry Measurements", *IEEE Transactions on Pattern Anakysis and Machine Intelligence*, vol. 22-18, pp. 1168-1171, 2000.

[22] L. Wang, G. Leedham, "*Near- and Far- Infrared Imaging for Vein Pattern Biometrics*", IEEE International Conference on Video and Signal Based Surveillance (AVSS'06), 2006.

Mohamed Khairy received his BSC and MSC in 2000, and 2005 from Department of Systems & Biomedical Engineering, Cairo University under the supervision of professor Ahmed Badawi. He is currently working as an engineer at Suez Canal Ismaillia Authority hospital. His research interests are in pattern recognition, image processing, and biometrics. He is a PhD student at Systems & Biomedical Engineering, Cairo University.

Ahmed Badawi (M'05-SM'06) received his BSC, MSC, PhD in 1990, 1993, and 1996 respectively from Department of Systems & Biomedical Engineering, Cairo University.

He was an assistant professor, associate professor, and full professor in 1996, 2001, and 2007 respectively at Systems & Biomedical Engineering Cairo University. He is a visiting professor at University of Tennessee, Biomedical Engineering Department since August 2005. He is a professor on leave at Systems & Biomedical Engineering, Cairo University. His research interests are in Medical Imaging, 3D/4D Ultrasound Scanning, Reconstruction, Visualization, and Measurements, 4D Surgical Navigation, Image Processing, Computer Vision and Pattern Recognition in Medicine, Neural Networks, Fuzzy Systems, Medical Classification, Biometrics, Intelligent Medical Systems, Medical Software Workstations. He is a reviewer of several international journals, chairman of several international conferences sessions and track chairman.

Dr. Badawi is a senior member, IEEE, a member in IEEE Engineering in Medicine and Biology society. Dr. Badawi published over 75 papers in journals and peer reviewed conferences. He awarded several prestigious awards such as Egyptian National Academy for Scientific Research and Technology, Cairo University award for Engineering Research. Dr. Badawi was a director of Imaging Solutions Department at ibetech.com where he was the head of the team who developed the first 3D ultrasound system in Egypt. Dr. Badawi has over 17 years experience in Systems & Biomedical Engineering teaching and research. Dr. Badawi supervised over 15 Msc and 2 PhD students.

Mohamed Kamel received his BSC, MSC, and PhD in 1982, 1985, and 1996 respectively, from Department of Systems & Biomedical Engineering, Cairo University. He is currently an assistant professor at Systems & Biomedical Engineering Department, Cairo University. His research interests are in pattern recognition, image processing, and biometrics. Dr. Kamel has several publications in international journals and peer reviewed conferences. Dr. Kamel has over 25 years experience in Biomedical Engineering teaching and research.